Journal of Polymer Research (2021) 28: 56
https://doi.org/10.1007/s10965-021-02418-z

ORIGINAL PAPER

Fabrication of polystyrene-acrylic/ZnO nanocomposite films for effective removal of methylene blue dye from water

Mariia Pasichnyk[1,2] · Miroslava Václavíková[3] · Inna Melnyk[3]

Received: 31 July 2020 / Accepted: 12 January 2021 / Published online: 21 January 2021

Abstract

Polymer nanocomposite films were formed from the aqueous dispersion of thermally linking styrene-acrylic copolymer (Tubifast 4010®, CHT), partially esterified melamine resin (Tubifix®, CHT), and ZnO nanoparticles as filler. The developed nanocomposite films were characterized by elemental (CHNS) analysis, SEM, EDX, IR spectroscopy, XRD, and swelling degree study. The EDX analysis proved the presence of Zn in the polymer nanocomposite, and according to SEM and XRD, all ZnO nanoparticles are separated with a uniform structure with 20 nm in size. Analyzing a swelling degree of the polymer films showed that the film with nano ZnO as the filler possesses 3.4 times lower swelling degree compared to the film formed from Tubifast 4010®. This can be explained by the inorganic structure of ZnO and the ability to form extra chains, which is consistent with IR spectroscopy data. It was demonstrated that the polymer nanocomposite film could adsorb methylene blue due to the quick swelling of the film which increases the volume of the sample and provides more active adsorption sites of the film.

Keywords Nanocomposites · ZnO nanoparticles · Styrene-acrylic polymer films · Melamine resin · Water treatment

Introduction

In the past few years, polymers with nanodimension fillers have captured the interest of scientists and technologists in water purification as they showed an ability to remove various pollutants like metal ions, dyes, and microorganisms. The most reasonable advantages that nanoparticles give to the polymer are improved processability, high values of surface area, stability, tunable properties, and cost-effectiveness [1].

Polymer nanocomposites are formed by blending inorganic nanoclusters with organic polymers, and polymer nanocomposite films can be formed by drying this solution. Besides, the inorganic nanoparticles can add to nanocomposites unique, optical, catalytic, magnetic, and electrical properties, while a polymer matrix can give mechanical and thermal stability to the films [2].

It has been realized that the higher concentration of free functional groups –COOH, $–NH_2$, –OH are beneficial to ionization and adsorption but their presence in polymer films results in excessive swelling or dissolution in an aqueous solution [3]. As a result, highly efficient adsorbents with metallic crosslinking multivalent ions, or ions with *d*-orbital and free electrons like Zn, Ti [4, 5], and functional ligands, such as –COOH, –OH were developed [6–8].

As it was shown polymer-metal or metal oxide nanocomposites are a new class of materials and now there is a strong focus on the methods of their controlled development with better-managed structure. In these cases, the process of creating nanomaterials usually consists of several stages, and for purposeful creation of composites, and their implementation in modern technology their structure on each stage of formation has to be controlled. Methods of the size and shape monitoring of the metal nanoparticles allow the modification of their properties and future characteristics. Chemistries and growth mechanisms of metal nanoparticles are very complicated, therefore it is still difficult to design and prepare particles with the preferred size and shape.

✉ Inna Melnyk
in.melnyk@gmail.com; melnyk@saske.sk

[1] V.O. Sukhomlynskyi National University of Mykolaiv, Mykolaiv, Ukraine

[2] Institute of Chemical Process Fundamentals, Czech Academy of Sciences, Prague, Czech Republic

[3] Institute of Geotechnics, Slovak Academy of Sciences, Kosice, Slovak Republic

Zinc oxide nanoparticles are commonly used metal oxides in polymer nanocomposites due to their low cost and favorable optoelectronic and catalytic properties. Nano-sized zinc oxide is more efficient at absorbing than the conventional size. In addition, it has good bactericide properties [9] and a high concentration of active sites. ZnO is characterized by highly efficient visible-light photocatalytic activity and generates large quantities of hydroxyl radicals. The vital role in the photocatalytic reactions plays surface and core defects. Such properties in ZnO as oxygen vacancies, oxygen interstitials, and zinc interstitials preventing electron–hole recombination and providing active sites forming [10]. The addition of ZnO nanoparticles in the structure of polymer film lets to create a new class of materials with improved mechanical properties, which are caused by the forming of three-dimensional structure with ZnO nanoparticles, and polymer network can prevent the releasing of Zn ions and let nanoparticle to be stable.

The electrons exchange or their transfer between adsorbent and adsorbate surfaces take place through the adsorption process and lead creation of stable chemical bonds [11, 12]. The adsorbents from polymer nanocomposites intense attention of the scientists, since it's become possible to regulate the morphology of their surface and their functional groups (such as –COOH, $–SO_3H$, $–NH_2$, –OH), which is decisive in the process of removing pollutants from the water, especially dyes [13,14,15].

Acrylates are commonly used as a component of polymer nanocomposites. The main properties are good adhesiveness, inexpensiveness, good film-forming properties, high block resistance, resistance to hydrolysis, hardness–softness, and resistance to UV light [16]. Also, they are suitable for adsorbents through ion exchange mechanisms, and as ion exchange resins, they characterized with efficient dye removal capacity [17]. In aqueous solution acrylic polymers have high water-absorption capacity due to the presence of hydrophilic carboxylate groups on the side chains, these groups have been certificated to be important for removing of cationic dyes [18].

There are many alternatives to applying polymer nanocomposites films for the treatment of wastewater contaminated with dyes with variable success to this date. These treatments include electrochemical degradation [19], cation exchange membranes [20], Fenton chemical oxidation [21], and photocatalysis [22, 23]. Adsorption is one of the high treatment methods for painted wastewater [24]. The excellent regeneration capacity of polymer nanocomposite films can be used for the uptake of, for instance, toxic dyes from wastewater [25]. Scientists from all over the world synthesized different types of polymer nanocomposites that used in water treatment: the composite consisted of clay and polyethylene (GCP) was used to remove methylene blue (MB) from the water [26]; ZnO/PMMA nanocomposites for photocatalytic degradation of phenol and methylene blue [27]; Graphene oxide-based polymer nanocomposites for the uptake of organic dyes from the aqueous solution [28]; in the work [29] was shown that the polymeric microspheres of amphiphilic block co-poly(arylene ether nitrile) exhibited highly selective adsorption for cationic dye MB due to the electrostatic interaction and π–π interaction; novel hydrophilic–hydrophobic optimized magnetic interpenetrating polymer networks (IPNs) of poly (methyl acryloyldiethylenetriamine)/polydivinyl benzene (PMADETA/PDVB) were synthesized by the interpenetration of polydivinylbenzene (PDVB) networks in the pores of the magnetic poly (glycidyl methacrylate) (PGMA) networks and used in water purification [30]. As it was reported all presented polymer nanocomposites had synergism between two components in composite leading to excellent adsorption properties for dyes removal. It is also possible to note such advantages of composite materials on the basis of polymers, as high adsorption capacity, mechanical strength, selectivity, suitable pore size, easy regeneration, and profitability [31]. The main disadvantages of the presented materials are the difficulty in obtaining polymer films with nanoparticles distributed in the polymer matrix and maintaining the basic properties of the components of the composition. On the other hand, no studies have been conducted explaining the structural features of the film based on polymers and inorganic nanoparticles and how the structure of polymer nanocomposite influence the absorption properties.

In the present work, the crosslinking system made from aqueous dispersions of sterol-acrylate partially substituted melamine, and ZnO nanoparticles, has been analyzed and used for the removal of Methylene Blue from the aqueous solution. MB has been chosen for this investigation because it is a water contaminant as a colorant agent for cotton, wool, and silk, and is a typical example of cationic dye. The exposure of MB in the human body may cause nausea, vomiting, jaundice, increased heart rate, profuse sweating, mental confusion, cyanosis, and quadriplegia [32]. The increase of dye pollutants is extremely dangerous due to the reduction the light transmittance, photosynthetic activity, and dissolved oxygen in the aquatic environment [33]. Therefore, the problem of dyes removing from water is an urgent task.

Materials

Synthesis of ZnO nanoparticles

ZnO nanoparticles were synthesized by direct precipitation method using zinc acetate ($Zn(CH_3COO)_2{\cdot}2H_2O$ (p.a., 99%, Centralchem, Slovakia) and sodium carbonate Na_2CO_3 (p.a., 99%, Centralchem, Slovakia). The synthesis was carried out using both 0.1 M ethanol (p.a., 99.8%, MikroCHEM) solutions of the above salts. The Na_2CO_3 solution was slowly added into

Scheme 1 The main components of polymer films

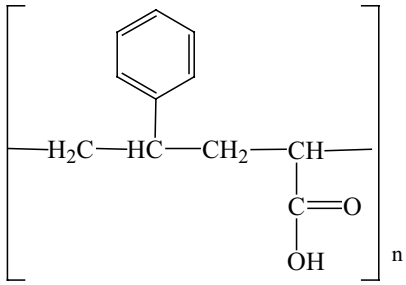

styrene-acrylic copolymer (Tubifast 4010®)

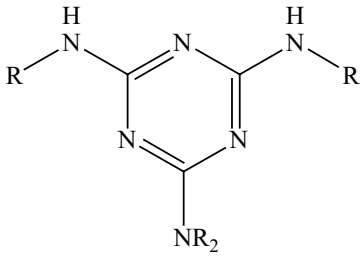

melamine resin (Tubifix®)

zinc acetate solution at room temperature under vigorous stirring, which resulted in the formation of a white suspension in ratio 1:1 (volume). The precipitate was centrifuged at 4000 rpm for 10 min and washed three times with distilled water. The obtained product was calcinated at 300 °C for 30 min.

$Na_2CO_3 + Zn(CH_3COO)_2 = 2Na(CH_3COO) + ZnCO_3$.

$ZnCO_3 \rightarrow ZnO + CO_2$.

Polymer nanocomposite films preparation

Aqueous dispersion of thermally linking styrene-acrylic copolymer (Tubifast 4010®, CHT, Switzerland: dry residue 45%, pH = 7−9, viscosity at 20 °C < 500 mPa·s) was used as a study object. Partially esterified melamine resin (Tubifix®, CHT, Switzerland: density 1.15 g/cm^3, pH = 8.5−10.5, viscosity at 23 °C 200 mPa·s) was used as a crosslinking agent (Scheme 1).

4 wt. % of crosslinking agent (Tubifix®) was added to the aqueous dispersion of Tubifast 4010®—polymer matrix (Scheme 2). The composition was stirred for 5 min on a magnetic stirrer. Zinc oxide nanoparticles in dry form were introduced into polymeric composition under vigorous mixing in an amount of 2 wt. %. The composition was mixed for 5 min and a homogeneous mixture was obtained.

Polymer compositions were poured into the Petri dish and dried at 80 °C for 60 min, heat treatment at 150 °C for 3 min (Scheme 2). The thickness of the studied composite polymer films was 0.05 mm; the films had no visible defects. The films containing only Tubifast 4010® or Tubifast 4010®+ Tubifix® were synthesized by the same method for comparison.

Characterization methods

Elemental analysis (CHNS) of total carbon, hydrogen, and nitrogen amount in obtained films was performed by elementary analyzer Vario MACRO cube (Elementar Analysen systeme GmbH, Germany). Helium and oxygen (99.995%, Messer, Austria) were used as the carrier and combustion gasses (intake pressures of 2 bars), respectively. Combustion tube was set up at 1150 °C, reduction tube at 850 °C, and sulfanilamide $C_6H_8N_2O_2S$ (Elementar, Germany) was used as reference standard.

The BET (Brunauer–Emmett–Teller) surface area was determined by low temperature nitrogen adsorption–desorption at -196 °C using Autosorb-6 adsorption analyzer (Quantachrome, USA).

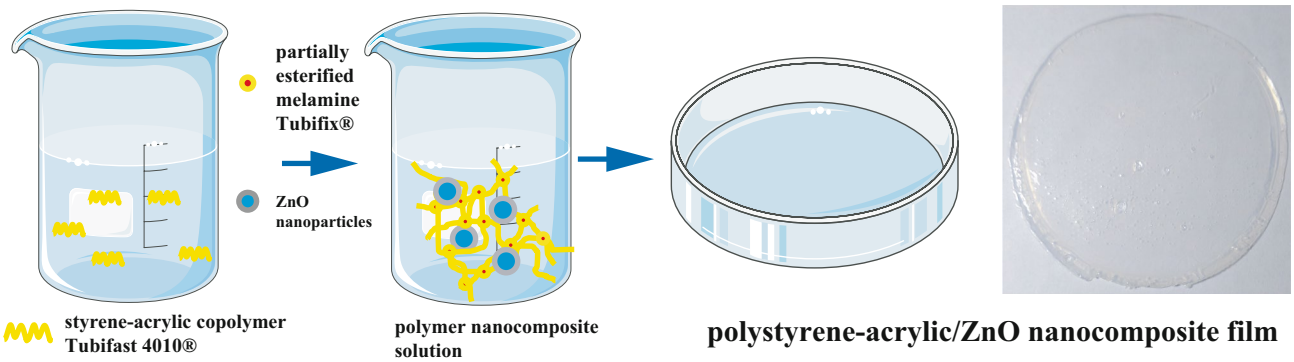

Scheme 2 Formation of polymer nanocomposite film

Fourier transform infrared (FTIR) spectra of the films were recorded with FTIR Spectrometer Tensor 27 (Bruker Optik GmbH, Germany) in the range of 4000–400 cm^{-1} with a resolution of 2 cm^{-1} in the reflection mode. For ZnO nanoparticles the pellet with KBr was formed, and the spectrum was recorded in the range of 4000–500 cm^{-1} in transmission mode.

Surface morphology of ZnO nanoparticles and composite films were studied by field emission scanning electron microscopy with MIRA 3 FE-SEM microscope (TESCAN, Czech Republic) equipped with a high-resolution cathode (Schottky field emitter), three-lens Wide Field OpticsTM design, and Energy-dispersive X-ray detector (EDX) (Oxford Instruments, UK). The samples were fixed on the objective table with previously deposited adhesion coating.

X-ray diffraction patterns for the ZnO nanoparticles and polymer films with nanoparticles were recorded using the Rigaku SmartLab® X-ray diffractometer using secondary monochromatic CuKα radiation of wavelength $\lambda = 0.1541$ nm at 40 kV/50 mA in the scan range $2\theta = 10°$ to 80°. Debye–Scherrer equation was used to calculate the average ZnO nanoparticles diameter:

$$D = \frac{0.94\lambda}{\beta cos\theta}$$

where β is the width (full-width at half-maximum) of the X-ray diffraction peak in radians and θ is the Bragg angle.

Photon cross-correlation spectroscopy analysis (PCCS analysis) was conducted on a Nanophox particle size analyzer (Sympatec, Germany) for ZnO nanoparticles water suspension to determine sample's particle-size distribution. The measurements were repeated three times for the sample.

The pH of the point of zero charge (pHzpc) was measured using the pH drift method. The pH of the polymer films in the 0.01 M NaCl solution was adjusted to between 2 and 12 by adding 0.01 M NaOH and 0.01 M HCl. 0.02 g of the polymer film was added to 5 cm^3 of the solution and after 24 h the final pH was measured.

The swelling experiment was conducted by the continuous method: a film with mass 0.05 g was immersed in a 50 cm^3 of water. After a definite swelling time, the sample was removed from the solution and the surface water was quickly removed with a filter paper. The sample was weighed and the weight was denoted as m_1 for the first immersion step. The sample was immersed in the solution for the second time, and the procedure was repeated until the equilibrium of swelling was reached.

Contact angle measurements were carried out using standard microscope equipped with the high resolution CCD camera (Sony SSC-C 370). 0.5 $cm^3$of de-ionized water scattered on the film surface were analyzed.

Sol–gel analysis of polymer film

The film samples were placed in the Soxhlet apparatus and extracted with acetone (p.a., 99.5%, Centralchem, Slovakia) during 18 h for the sol–gel analysis of polymer films. The films were dried in a thermostat at 60 °C for 2 h and held at room temperature for 30 min.

The samples were further extracted with benzene (p.a., 99.7%, Lachema, Czech Republic) in another Soxhlet apparatus for 16 h. The films were weighed after extraction with acetone and benzene. The amount of benzene extract (in %) corresponded to the content of the sol fraction *S*:

$$S = \frac{m_a - m_b}{m_a} 100\% \quad (1)$$

where: m_a—mass of the sample after extraction in acetone, g; and m_b—mass of the sample after extraction in benzene, g.

The swelling process is characterized by the swelling degree that was determined by formula:

$$a = \frac{m_2 - m_1}{m_1} 100\% \quad (2)$$

m_1 – mass of the sample after swelling in benzene, g; m_2 – mass of the sample before extraction, g.

Fraction of moist-free polymer in the swollen gel was determined by the formula:

$$V_r = \frac{1}{a} \quad (3)$$

Polymer cross-linking degree was determined by an experimentally derived number of sol fraction (*S*) for each film:

$$j = \frac{1}{S + \sqrt{S}} \quad (4)$$

Fraction of active chains that are capable for cross-linking reaction was calculated by formula:

$$V_c = (1 - S)^2(1 - jS)(1 + jS) \quad (5)$$

Methylene blue adsorption experiments

Adsorption study was carried out with 0.03 g of the polymer film added to 25.0 cm^3 (300.0 ppm solution) of cationic dye MB (95%, MicroCHEM, Slovakia) at pH ~6.0 in a static mode. Samples were collected after 24 h, and the MB absorbance was measured at 664 nm on a Helios Gamma UV–vis spectrophotometer (Thermo electron corporation, UK).

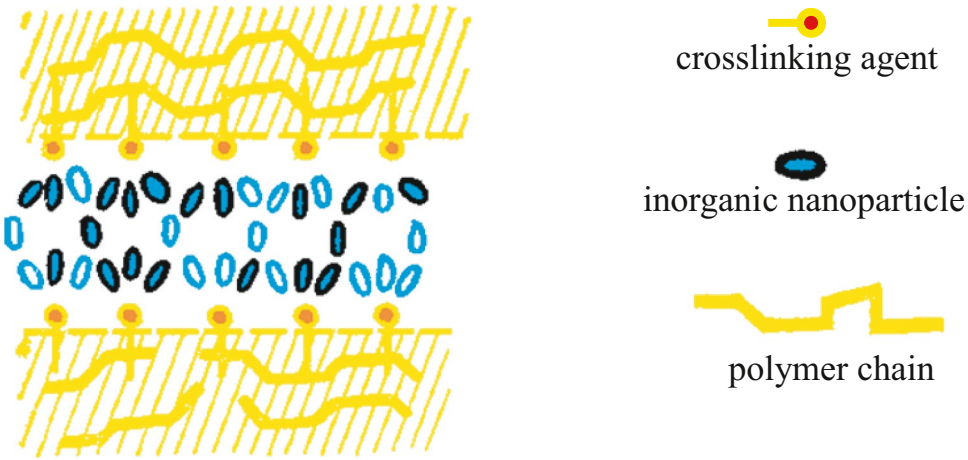

Scheme 3 Crosslinking in polymer film with inorganic nanoparticles

Results and discussion

Study of crosslinking in polymer nanocomposite films (Sol–gel analysis)

Theoretical and experimental studies show that inorganic particles with high geometric factors have the significant enhancement effect when they are injected into the polymer matrix. Inorganic nanoparticles lead to improved mechanical properties, as a result of the increasing crosslinking in composites with elastomer binder (Scheme 3).

Since intermolecular cross bonds are formed by cross-linking, the linear or branched structures develop into a three-dimensional polymer network that is unable to dissolve and melt. Therefore, the primary research method to determine the extent of polymer cross-linking is the theory of Flory-Raineri, based on the equilibrium swelling and connecting the number of the net active chains with the relative polymer fraction in the swollen system [34, 35]. The crosslinking theory enables to predict the relationship among molecular parameters characterizing polymer nanocomposite films such as crosslinking density, gel point, sol fraction, degree of polymerization, and molecular weight distribution of sol molecules.

Table 1 shows that films based on styrene-acrylic polymer Tubifast 4010® are distinguished by a high degree of intermolecular cross-linking. Taking into account that the individual Tubifast 4010® film is unstable to solvents, the introduction of crosslinking agents increases the degree of the structuring of the polymer. The 4% concentration of Tubifix® as the crosslinking agent decreases a fraction of the active chains in 5 times, which results in the significant increase in the crosslinking density of the polymer film. Adding nano zinc oxide as the filler to the polymer composition, a degree of crosslinking increased almost fourfold. The fraction of active chains decreased ~ 82 times.

The styrene-acrylic polymer features presence of long flexible sections of molecules separated by carboxyl groups, which contribute to the strong local interaction between chains resulting in the formation of linear structures (Scheme 4). The presence of carboxyl groups of methacrylic acid in the acrylic copolymer provides the formation of an elastic polymer structure.

When self-linking in styrene-acrylic polymers takes place (Scheme 4), not all carboxyl groups react. Therefore, admixtures of free acid monomers are deliberately added in the industrial production of styrene-acrylic polymers to achieve a maximum degree of interaction of the polymer with crosslinking agents. A crosslinking agent (partially etherified melamine resin) was added in order to increase the crosslinking degree in the styrene-acrylic polymer (Scheme 4). In this case, the interaction between the carboxyl groups of styrene-acrylic polymer and methylene groups of the crosslinking agent is formed and a strong grid-type structure arises [36, 37]. The introduction of crosslinking agents into the polymer composition provides the formation of a three-dimensional spatially "stitched" structure. However, free -NH_2 groups increase the resistance to non-polar solvents, nano ZnO

Table 1 Sol–gel analysis of polymer films

Polymer film	Sol fraction *S*, %	Cross-linking degree *j*,%	Fraction of active chains V_c	Swelling degree *a*, %	Fraction of moist-free polymer in the swollen gel V_r
Tubifast 4010®	43.08	2.01	2433.98	14.05	0.07
Tubifast 4010®/ Tubifix®	21.59	3.81	499.13	4.36	0.22
Tubifast 4010®/ Tubifix®/Nano ZnO	4.34	15.54	6.60	4.13	0.24

Scheme 4 Scheme of interactions during composite formation

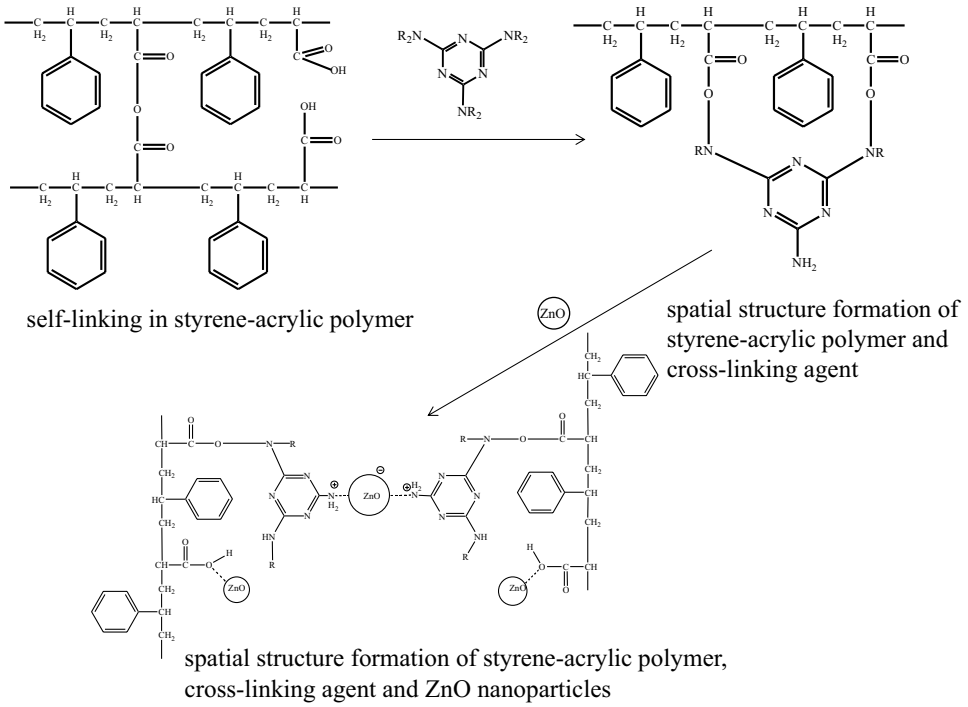

was added to polymer composition as a filler blocking these groups (Scheme 4).

ZnO nanoparticles create a three-dimensional cross-linked structure forming a polar linking between -NH_2 groups and ZnO nanoparticles. This can explain the high stability of such film in organic solvents, and predict a good possibility to use such films for water treatment purposes. Also, we suppose that free –COOH groups of the styrene-acrylic polymer can react with the ZnO nanoparticle core due to the van der Waals force and electrostatic force. These interactions can explain the increase of the cross-linking degree in 6.5 times.

Investigation of polymer films composition by elemental analysis and FTIR

The development and production of polymer nanocomposites require quality control of raw materials and additives. The analysis of the behavior of polymers and nanoparticles during molding and the evaluation of their lifetime contributions to define their quality. For the material characterization and the quality control testings of the presents of nitrogen, carbon, hydrogen, sulfur, and oxygen are determined.

Content of nanocomposite films was studied by elemental analysis (Table 2), an exact percentage of the organic components of the polymer films was established. It was summarized, the element ratios were C/H = 7.2 and C/N = 38.8 in the polymer film with ZnO nanoparticles.

All the samples consist of the small amount of Nitrogen, which is used to trigger a polymerization reaction. For the specific properties in water purification presence of Nitrogen was increased by adding a cross-linked agent that acts as the emulsion stabilizer for polymers nanocomposition, chain transfer agent, plasticizer to increase flexibility, a stabilizer to prevent polymer degradation, and an ingredient to modify polymer networks.

In addition, both the composition of the raw components and composites were determined by IR spectroscopy. The FTIR spectrum of ZnO was recorded in transmittance mode, and it is given in Fig. 1a: the broad band at 3424 cm^{-1} is corresponding to the stretching vibration of O–H groups as well as the absorption band at 1400 cm^{-1} is due to the O–H bending of alcohol residues; the band at 416 cm^{-1} is attributed to the Zn–O stretching vibration which is consistent with the previously reported work, 1575 cm^{-1} (bending) indicates the presence of hydroxyl residue which is due to atmospheric moisture [38].

The network structure of polymer film was confirmed as well (Fig. 1b-c). Figure 1b presents the infrared spectrum of polymer matrix Tubifast 4010®. It includes all the characteristic

Table 2 Elemental analysis of nanocomposite polymer films

Sample	Elemental analysis data, mass.%			
	Carbon	Nitrogen	Hydrogen	Oxygen
Tubifast 4010®/ Tubifix®	65.15	3.54	9.34	21.97
Tubifast 4010®/ Tubifix®/ Nano ZnO	64.78	3.54	9.32	22.36

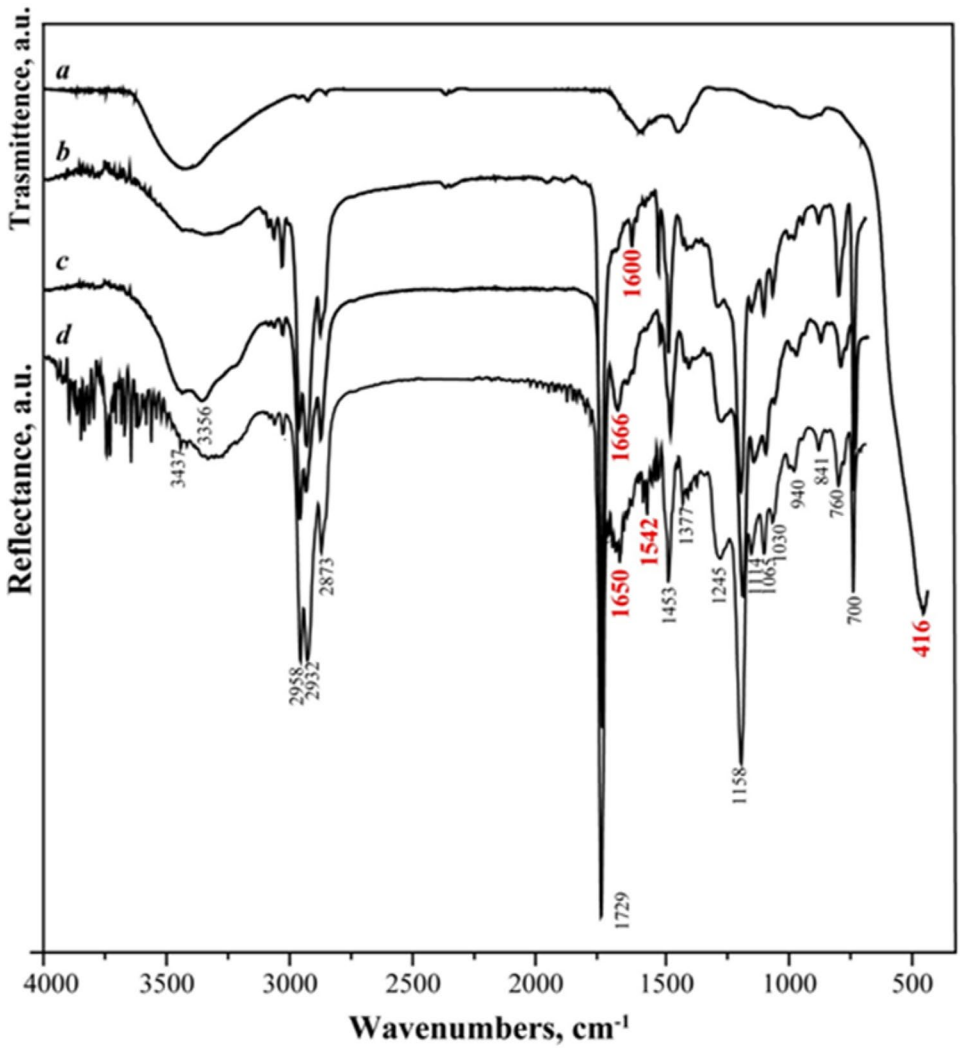

Fig. 1 FTIR spectra of ZnO nanoparticles **a**, polymer matrix Tubifast 4010® **b**, polymer nanocomposite film with ZnO nanoparticles **c**, polymer nanocomposite film after adsorption of MB **d**

absorption bands for the styrene-acrylic polymer. Thus, the absorption bands at 2958, 2932 and 2873 cm^{-1} are referred to asymmetric and symmetric C-H vibrations of alkyl groups; the low-intensive absorption band at 3027 cm^{-1} is corresponded to = C-H stretching vibrations of the phenyl ring of styrene together with the low-intensity band at 1600 cm^{-1} which is referred to stretching vibrations of the C = C in the benzene ring; the intensive sharp band at 1729 cm^{-1} belongs to the C = O vibrations of carboxyl groups in copolymer; the intensive band at 1453 cm^{-1} is due to bending vibrations of -CH_2 groups; the band at 1158 cm^{-1} corresponds to stretching vibrations of C–O–C, which indicates the self-cross-linking in the polymer due to the etherification of carboxyl groups.

Figure 1c shows the infrared spectrum of polymer nanocomposite film with ZnO nanoparticles. The absorption bands in the range 3500–3300 cm^{-1} are referred to the stretching vibration of -NH_2 groups of Tubifix® crosslinking agent as well as the absorption band of deformation vibrations of amino groups at 1666 cm^{-1}. The composite film has the typical C–N vibrations at 1030 cm^{-1} is attributed to the melamine structure of Tubifix®. On the spectrum, we can recognize the stretching vibrations of O-C in the carboxyl group at 1245 cm^{-1} indicating the formation of a three-dimension structure. However, the presence of ZnO nanoparticles in the composite film was not proved because of another mode of the spectrum recording from 500 cm^{-1}, but their presence is proved by other methods below.

Exploration of polymer films morphology and ZnO size by SEM, PCCS, and XRD

SEM micrographs of the inner and surface structure offer remarkable figures about the morphology of the obtained films. Quite clear can be seen surface smoothness, layer structure, and cracks. It is shown the surface of the film based on Tubifast 4010® (Fig. 2a) consists of big parts

of non-dissolved polymer this phase can be seen sufficiently clear. The film based on the composition of Tubifast 4010® and Tubifix® demonstrates varying amounts of voided "multi-layer-like" structures exhibiting fracture lines perpendicular to the film surface (Fig. 2b). The morphology of polymer films with ZnO nanoparticles characterized by a fine oriented structure without voids (Fig. 2c). The SEM images indicate the homogeneous dispersion of ZnO nanoparticles. The absence of defects in the matrix and on the film surface is indicative of the structural integrity of the matrix, which could explain the better cross-linked degree of the obtained film (Fig. 2d).

As expected, the polymer films are non-porous materials with low specific surface values (18, 1 and 9 m^2/g, respectively). It can only be noted that for the sample with the crosslinking agent there is a hysteresis loop, which indicates the presence of some pores or holes.

SEM image of the obtained ZnO nanoparticles (Fig. 2e-f) and the particle-size distributions plotted using the PCCS analysis are depicted in Fig. 3. Combining photon cross-correlation spectroscopy and SEM, more accurate information about the particles' sizes was obtained. The SEM images show agglomerations of individual zinc oxide particles. A closer look at the agglomerated lump (Fig. 2f) shows the presence of several nanoparticle aggregates. In Fig. 2e particles appear to be agglomerated and some individual crystals are clearly visible. According to photon cross-correlation spectroscopy (Fig. 3), the sample consists of 45–50 nm particles in size. Analyzing the SEM image the particles are marginally agglomerated but the particle separation is not good enough here also we can see that the particles are held together in the solid phase because of weak physical forces, but in the liquid phase particles don't form agglomerates. SEM image of ZnO nanoparticles and the distribution of the particles matched with other researches [39, 40].

Synthesized nanoparticles were investigated by X-ray diffraction. The pattern of ZnO nanoparticles shows that the diffraction peaks located at 31.8°, 34.44°, 36.32°, 47.6°, 56.71°, 62.96°, 68.13° and 69.18° have been clearly indexed as hexagonal wurtzite phase of ZnO (JPCDS card no: 36–1451). It also ratifies that nanoparticles were

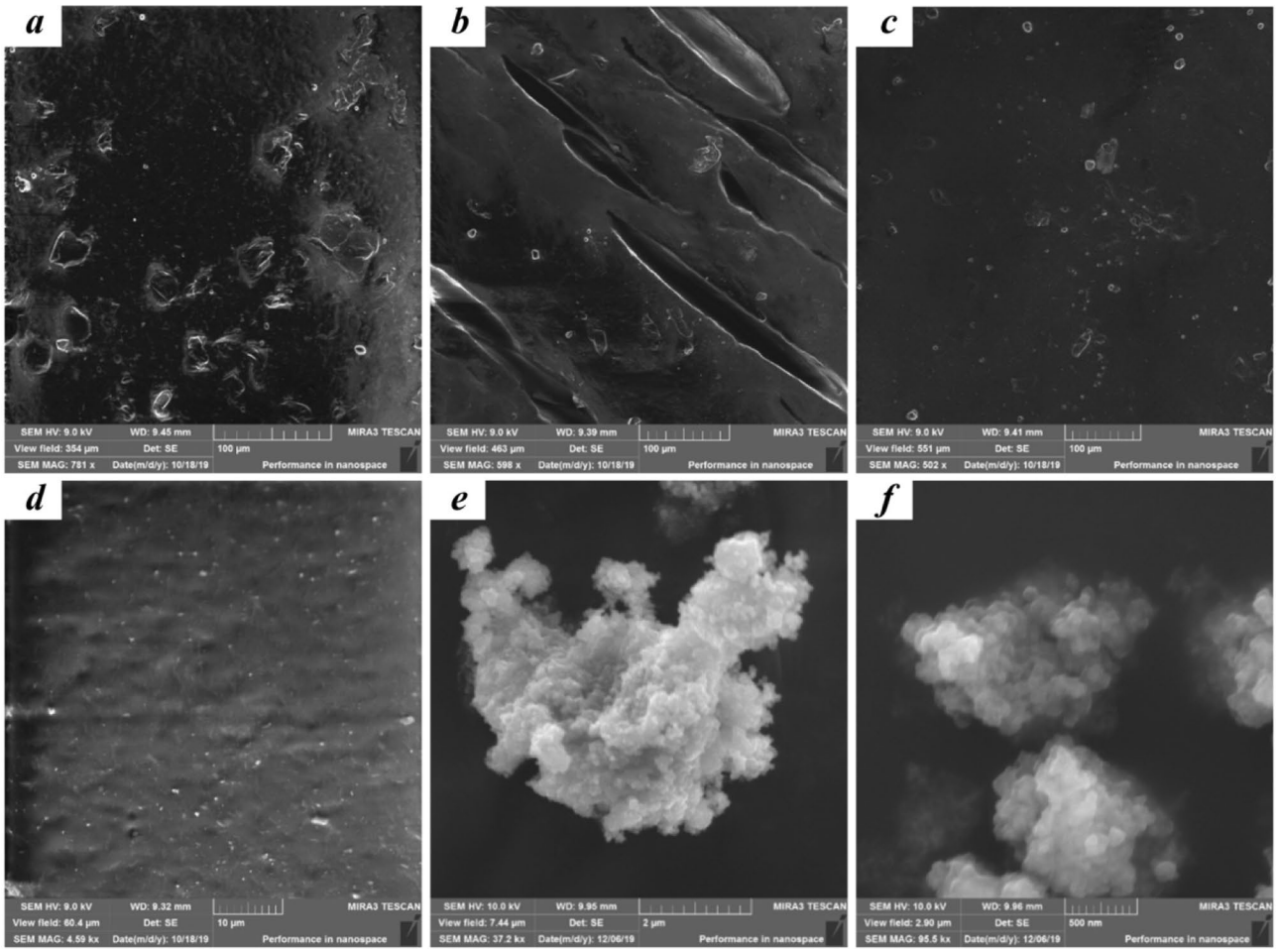

Fig. 2 SEM images of: the film based on Tubifast 4010® **a**, the film Tubifast 4010®/ Tubifix® composition **b**, the composite film Tubifast 4010®/ Tubifix®/nano ZnO **c**,**d**, ZnO nanoparticles **e**,**f**

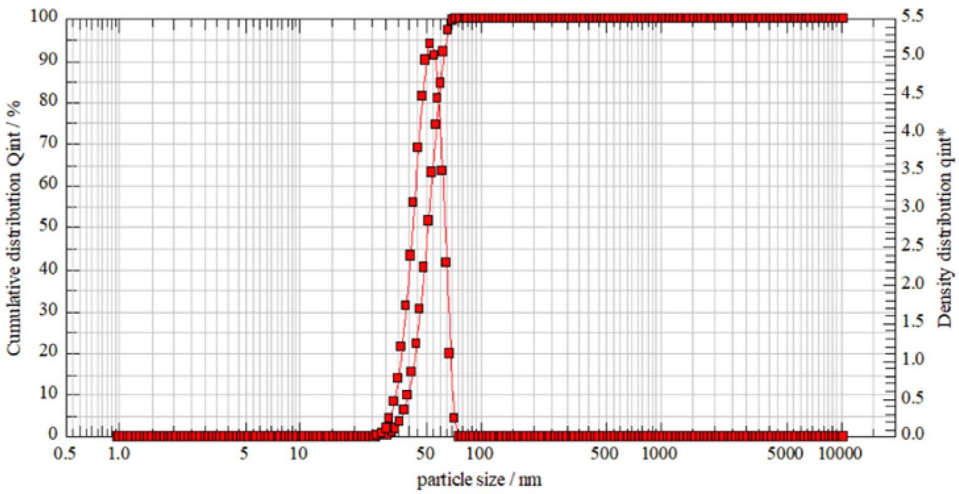

Fig. 3 ZnO particle size distribution based on photon cross-correlation spectroscopy data

impurity-free as it does not contain any characteristic XRD peaks other than ZnO peaks. Nanoparticles possess good crystallinity which is shown by strong and narrow diffraction peaks.

The average particle size of the samples calculated from the Debye–Scherrer equation was 40 nm, the plane (101) is found to be more intense than other peaks. These data correlate with the data obtained by PCCS (Fig. 3). When ZnO nanoparticles are involved in polymer composition the diffraction peak intensity is decreased and shifts of approximately 1° in the peak positions. The diffraction peaks broadening in the XRD pattern indicates the presence of microstrain in the respective sample. This possible change in the peak intensities is due to the change in the electronic density in the crystallographic position. The Fig. 4 shows the shift in the XRD peak positions of ZnO towards the higher values, demonstrating the existence of tensile strain in the sample.

Otherwise, the addition of ZnO nanoparticles to the polymer matrix prevents their aggregation. Nanoparticles are distributed in the polymer matrix, all respective ZnO peaks have the same position. The size of the nanoparticles in the polymer nanocomposite film is 20 nm. The intensive peak locked at the 20° (Fig. 4b) confirmed the amorphous structure of the polymer.

The EDX spectrum proves the presence of Zn and O in the polymer nanocomposite. As shown in Fig. 5 all nanoparticles are separated with uniform structure, nanoparticles mostly don't aggregate and lump tightly than precise ZnO. This might be owing to the polymer chains performing as folders in the composite, which hold together or lump the composite particle together. Moreover, the ZnO particles are determined to be captured in the polymer matrix. These outcomes expose that the ZnO particles are not merely mixed up or merged with the polymer, signifying that the ZnO particles are implanted in the polymer

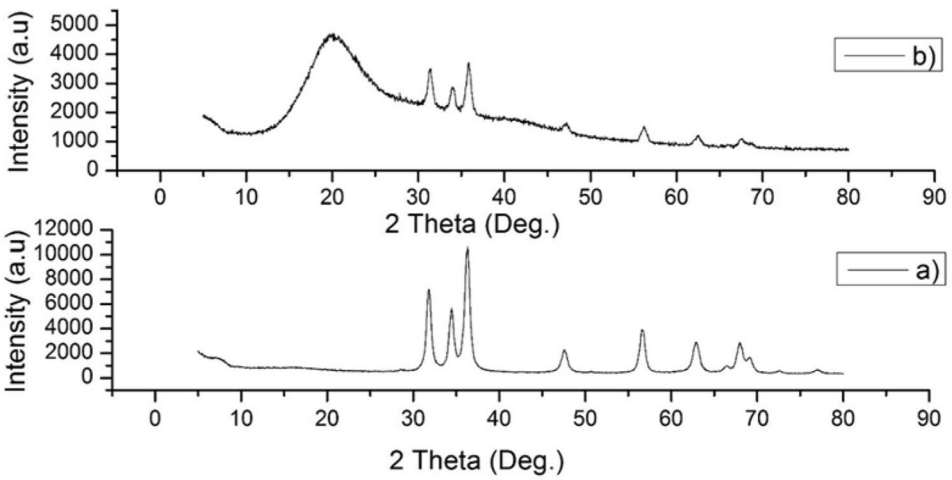

Fig. 4 XRD patterns: **a** ZnO nanoparticles; **b** polymer nanocomposite with ZnO nanoparticles

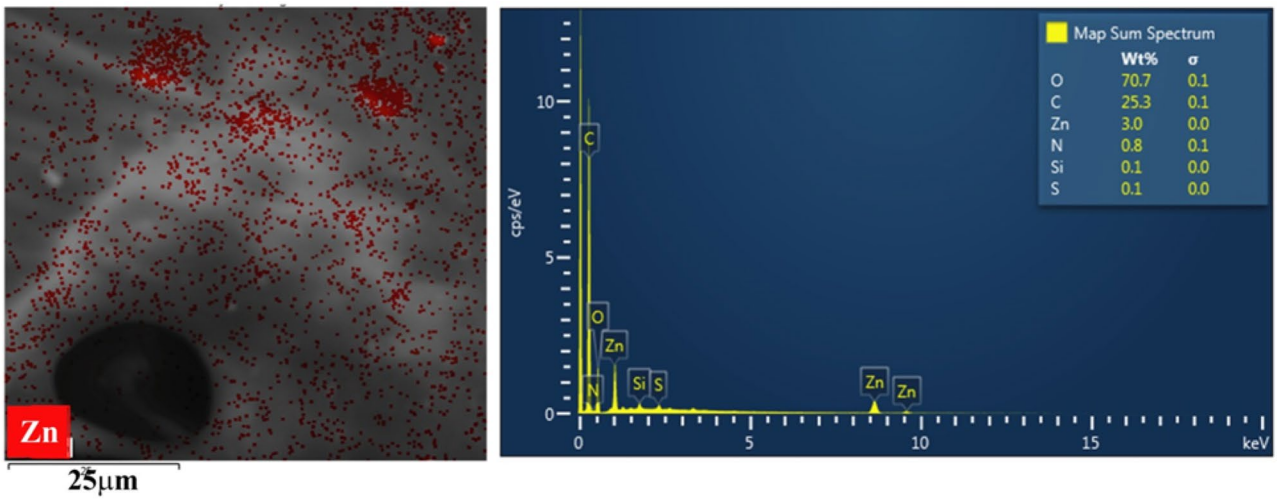

Fig. 5 SEM image of nanocomposite and its EDX spectrum

matrix, which is fairly in conformity with the outcomes of the XRD analysis (Fig. 4b) [41].

Estimation of the polymer film surface point zero charge

In order to determine the charge of the adsorbent surface, the Point of Zero Charge (Pzc) was measured (Fig. 6). For instance, pHpzc for sterol-acrylic polymer film Tubifast 4010® and polymer film with crosslinked agent Tubifix® was around 7.00. That means that at the pH below Pzc, the surface is charged positively. The surface of polymer film with ZnO nanoparticles was more basic and shifted to higher values pHpzc = 9.04. Increasing the pH of the polymer film indicates an increase in the concentration of OH^- ions in the solution, it is likely that H^+ ions are adsorbed on the film surface. Therefore, we can conclude that under these conditions the polymer nanocomposite film exhibits basic properties. According to these results, we can confirm that polymer film based on Tubifast 4010® and Tubifast 4010®/ Tubifix® shows the absence of active groups (-COOH or $-NH_2$) on the surface, as all groups are cross-linked. Adding to polymer composition ZnO nanoparticles results in the appearance of $ZnOH^+$ on the surface,

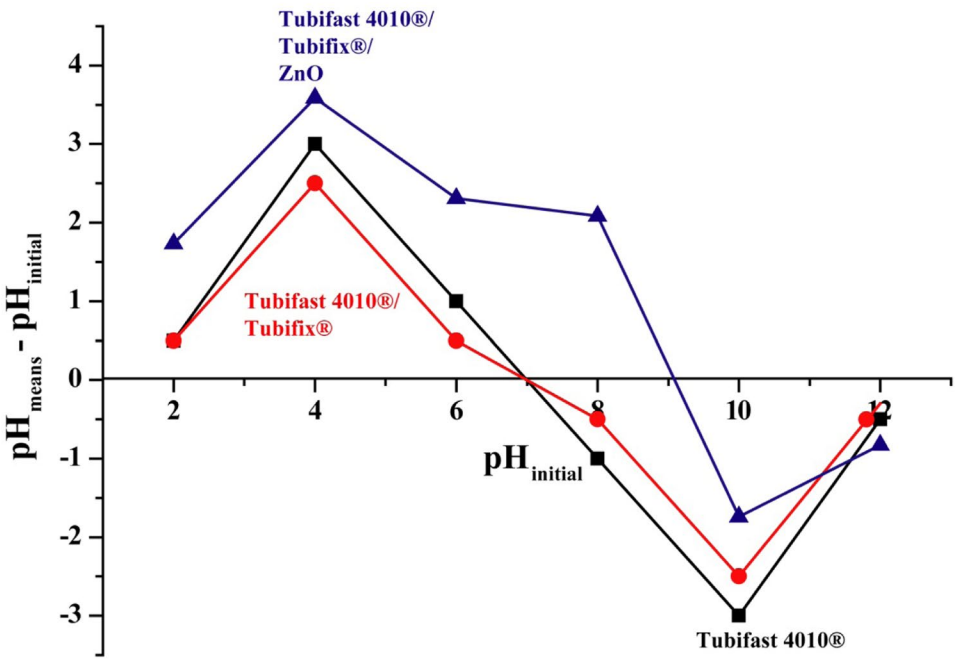

Fig. 6 Point of Zero Charge of the polymer films

which can react with -NH_2 groups of melamine [42] as the surface become more basic.

Examination of water resistance of the polymer films

The polymer films' swelling was studied under the conditions of the adsorption experiment mainly due to the fact that the polymer films swell in aqueous solutions. Swelling analysis demonstrates the water uptake by the samples during the time. Changes in the swelling ratio of the polymer films are shown in Fig. 7, and the water uptake increases with time for all the samples. The biggest swelling capacity demonstrates polymer film based on Tubifast 4010®/ Tubifix® (270%), adding the cross-linker to the polymer film increases the swelling ratio, which could be due to the more bonds formed by the cross-linking process. Slightly less degree of the swelling showed Tubifast 4010® polymer film (246%) compared to dried one. The polymer film with ZnO nanoparticles owns the biggest crosslinking degree 15.54% (Table 1), therefore in water solution, this film showed the lowest swelling (215%) compared to the dry film.

Thereby, the swelling ratio of the samples is in the range of 50 to 300%, which is comparable with other polymer films. Polymer film with ZnO nanoparticles shows the decrease in the water uptake by 12.6% in comparison to other samples and could be introduced as the promising adsorbent.

The nature of hydrophobic-hydrophilic groups on the surface of the films was determined by the contact angle measuring almost immediately after water drops deposition (within 3–5 s) (Fig. 8). All polymer films are characterized by a low water contact angle ($\theta < 90°$), which indicates high hydrophilicity and good wettability. Comparing these results for the polymer samples we can conclude that the hydrophilicity was improved by the ZnO nanoparticles addition to the composition.

Testing of the films for methylene blue adsorption

The polymer films were tested in the removal of MB from aqueous solution as a basic cationic azodye. After dissolution, the chloride ions enter the aqueous solution, providing the positive charge above the dye [43].

The dye adsorption tests were conducted to show the advantages of polymer nanocomposite film compared to the film without ZnO nanoparticles in such processes. Figure 9 presents UV–vis spectra and comparative characteristics of MB solutions before and after adsorption. As can be seen, the MB adsorption by the polymer film with ZnO nanoparticles is higher than by the film without nanoparticles. Swelling of the polymer film increases the polymer volume, which results in more active adsorption sites on the film.

The polymer film Tubifast4010® can adsorb the MB via the hydrophobic π–π interactions between the aromatic rings of the dye and the sterol-acrylate matrix. The polymer film with cross-linked agent Tubifix® demonstrates

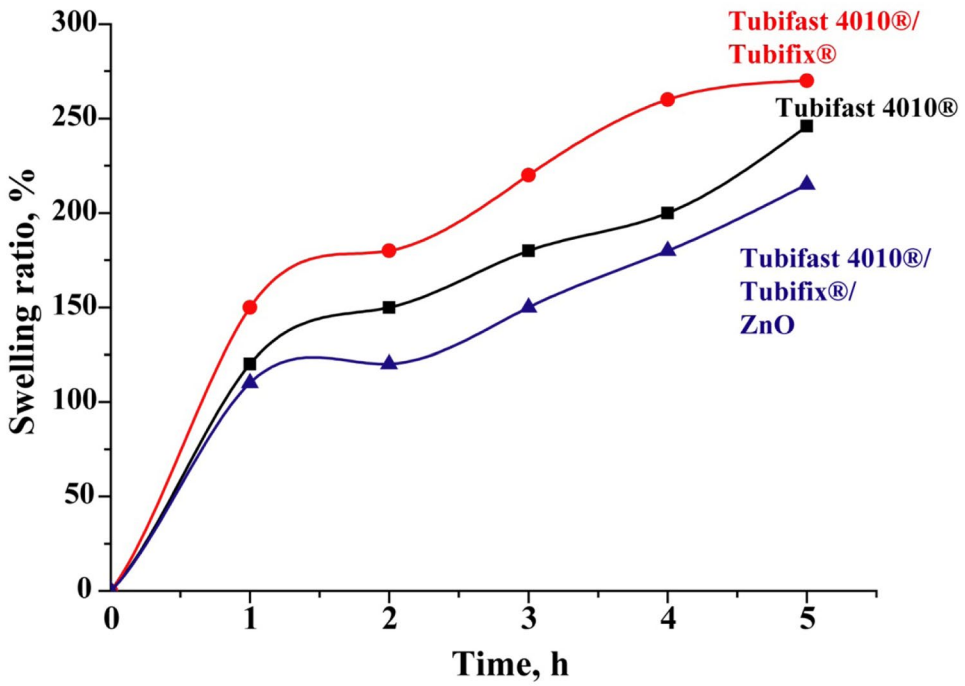

Fig. 7 Changes in the swelling ratio of the polymer films

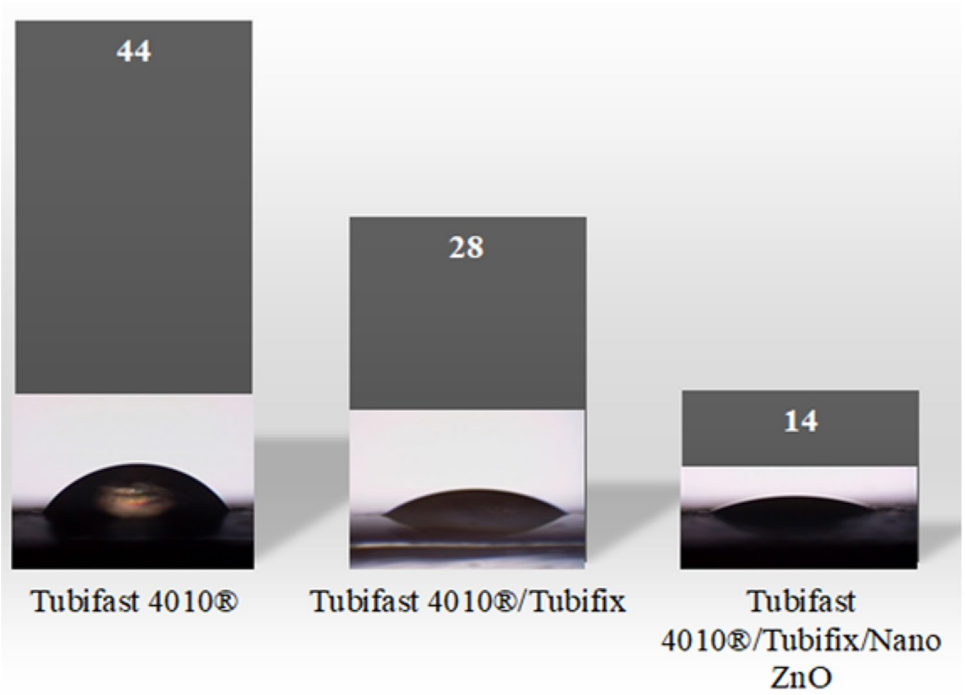

Fig. 8 Differences in contact angles between polymer films

a higher sorption capacity due to the ion exchange mechanism by forming of H-bondings, which can be created between the nitrogen of the amino groups of MB and nitrogen of the -NH_2 group of melamine in Tubifix® structure as well as the oxygen of the carbonyl group of the sterol-acrylate. It was recognized that as the MB anions are too large, they are excluded because of the 'sieve effect' in the polymer film. Adding of ZnO nanoparticles as filler to the polymer film makes adsorption capacity much higher, the ions MB could be easily adsorbed on the surface of polymer nanocomposite film by electrostatic attraction too. The amount of methylene blue increases on the surface of

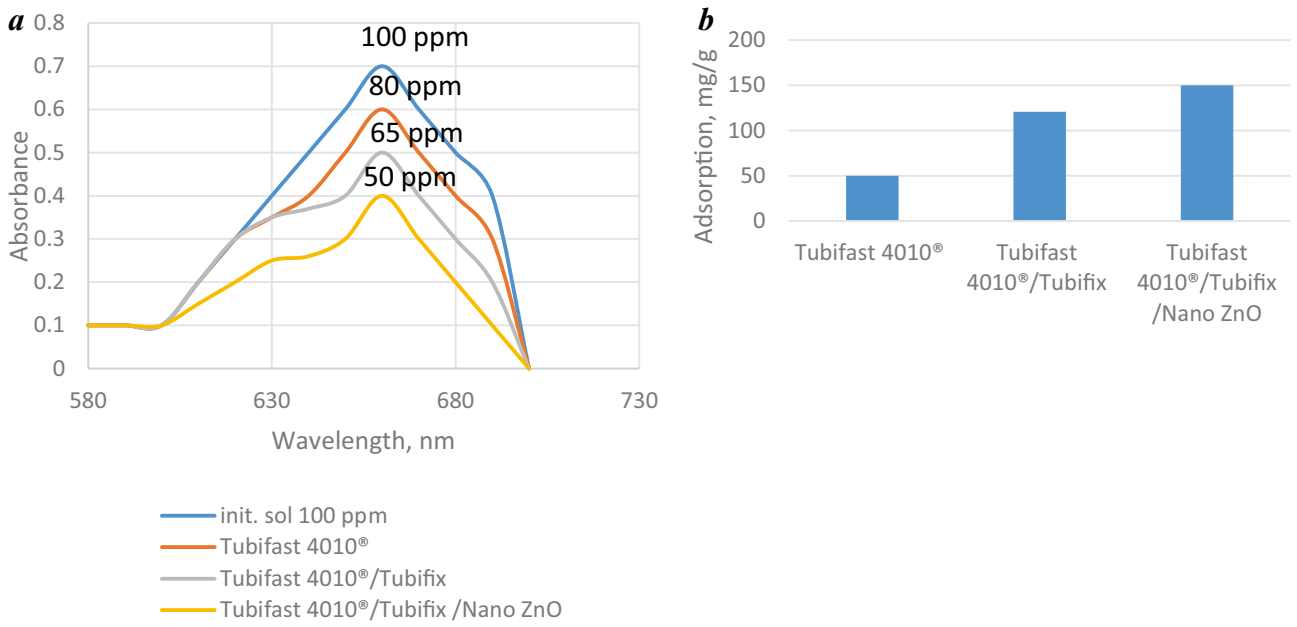

Fig. 9 UV–Visible spectra of methylene blue initial solution and solutions after adsorption (diluted in 25 times) **a**; quantity of MB that can accumulate on the surface of the polymer films **b**

Scheme 5 Proposed mechanism of adsorption methylene blue by polymer nanocomposite film

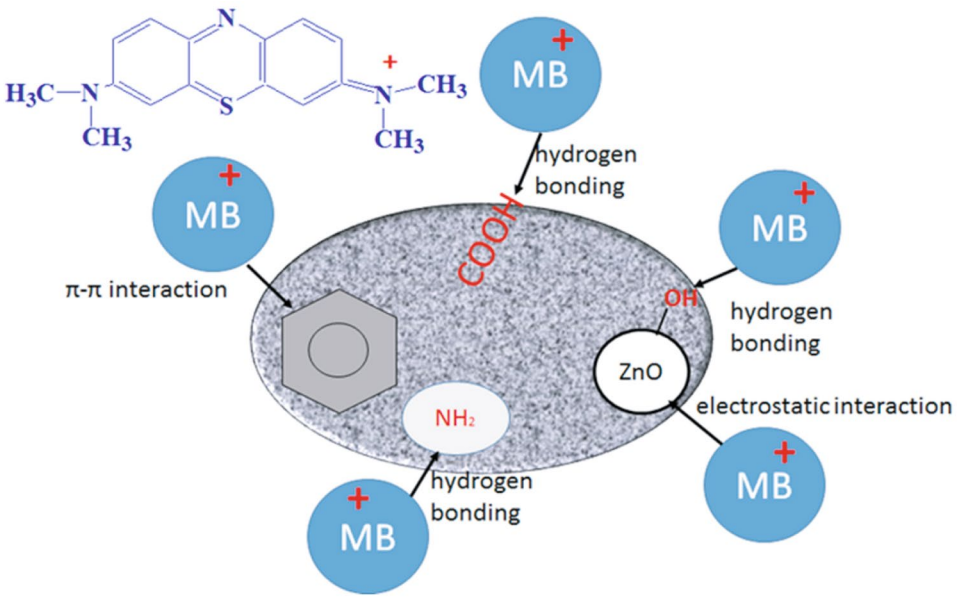

polymer film due to the ion exchange mechanism of the sterol-acrylate matrix (Fig. 9b).

The surface chemistry of the polymer film before and after MB adsorption was analyzed (Fig. 1c, d) using IR spectroscopy. The absorption bands involved in the adsorption of MB include the band centered at 3437 cm^{-1} associated with the stretching vibration of hydroxyl groups. Figure 1d shows changes in IR spectrum of polymer film after MB adsorption such as: the band shift from 1666 cm^{-1} to 1650 cm^{-1} for bending vibrations of amino groups; as well as the disappearance of stretching vibrations of amino groups in the region 3300–3400 cm^{-1}, which indicates the interaction of MB with these groups of polymer nanocomposites; the band at 1542 cm^{-1} associated with C = C vibration indicates an increase in unsaturated substances on the surface of the film. Also, these shifts may specify the interaction of the dye with nanoparticles of zinc oxide, if the ZnO nanoparticles were surrounded by amino groups (Scheme 4) and participated in the adsorption of MB.

To sum up, two mechanisms occur during the adsorption of methylene blue in polymer film. First, physical (π-π stacking interaction between MB and aromatic rings of the polymer) and the second, chemical (hydrogen bonding between MB and –COOH, $-NH_2$, -OH groups of the polymer and electrostatic interactions with ZnO nanoparticles). Probably the sharing/transfer of electrons between the adsorbate and adsorbent due to the electron-rich N and Zn atoms occur in the nanocomposite film. This result was consistent with the analysis of the material by FTIR, which showed that organic functional groups obviously shifted after MB adsorbed onto the surface. Therefore, organic functional groups of polymer composition played an important role during the MB adsorption. The recommended mechanism is displayed in Scheme 5.

The oversaturated MB is absorbed onto the surface of polymer nanocomposite film (Fig. 10). Results of adsorption properties indicated that this composite material is characterized by high sorption capacity (150 mg/g). Comparing

Fig. 10 Removal of MB from water by the composite film in the laboratory

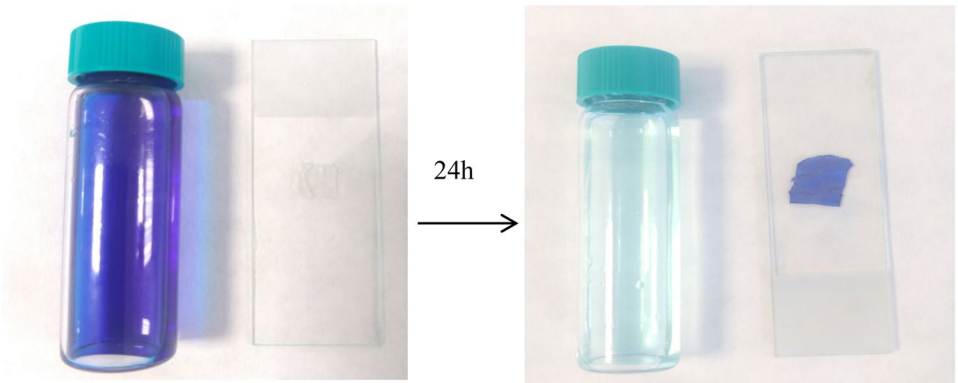

the other materials used for MB removal, the obtained polymer composite in this research could be applied as an efficient adsorptive material, for example: polymer hydrogel G-1–4 (342.9 mg/g) [7], MoS_2 polymer composite MoS_2-PDOPA (244.03 mg/g) [11], carbon material CAC (149.25 mg/g) [24], graphene oxide-magnetite composite GO-Fe_3O_4 (172.6 mg/g) [28], amphiphilic block co-poly(arylene ether nitrile) microsphere B-*b*-S-P (119.84 mg/g) [29], zinc-doped cobalt ferrite $CoFe_{1.9}Zn_{0.1}O$ (27.79 mg/g) [32], magnetite nanoparticles with polysilsesquioxane bearing HS-complexing groups BM-4 (88 mg/g) [44], aminosilica particles with phenyl groups TAPh 6–1-1 (99 mg/g) [45], and mesoporous magnetic silica composite MMSC (115.2 mg/g) [46].

Conclusion

The composite film based on the styrene-acrylic dispersion, the melamine crosslinking agent, and ZnO nanoparticles as the filler was developed. According to SEM, EDX, and XRD studies, it is obvious that the diameter of ZnO nanoparticles could be reduced by adding them to polymer composition thereby their aggregation could be prevented. It was shown that the individual polymer films formed from styrene-acrylic polymer Tubifast 4010® are not able to provide quality characteristics to a polymer film, and therefore require the addition of crosslinking agents. It was determined that the film based on styrene-acrylic polymer, crosslinking agent, and nano ZnO offers the high degree of intermolecular cross-linking and lower swelling in water and benzene, due to the forming of extra chains in the film structure. Interactions between active chains of the components of polymer composition were demonstrated and proved by FTIR, XRD, SEM, EDX techniques. Polymer nanocomposite film with ZnO nanoparticles distinguished themselves as promising adsorbents for the removal of methylene blue from the wastewater. The value of the adsorption of cationic MB is almost 2 times higher than for similar films without nanoparticles. The FTIR analysis of polymer film before and after the adsorption of MB allows concluding that the dye had effective interactions with the functional groups of nanocomposite film.

Acknowledgement The authors are grateful for the financial support from SAIA, n.o. within National Scholarship Programme of the Slovak Republic, APVV-19-0302 and VEGA 2/0156/19 projects, Czech Science Foundation grant N°19-08153Y. As well RNDr. Jana Gaálová, Ph.D. (Institute of Chemical Process Fundamentals, Czech Academy of Sciences) is acknowledged for contact angles measurements.

References

1. Malaviya P, Singh A (2011) Crit Rev Environ Sci Technol 41:1111. https://doi.org/10.1080/10643380903392817
2. Pandey N, Shukla SK, Singh NB (2017) Nanocomposites 3:47. https://doi.org/10.1080/20550324.2017.1329983
3. Zheng P, Xu M, Liu X, Jia K (2018) Solid State Ion 316:110. https://doi.org/10.1016/j.ssi.2018.01.002
4. Kang D, Liu Q, Chen M, Gu J, Zhang D (2016) ACS Nano 10:889. https://doi.org/10.1021/acsnano.5b06022
5. Zhou X, Jia K, He X, Wei S, Wang P, Liu X (2018) J Mater Sci-Mater El 29:8380. https://doi.org/10.1007/s10854-018-8849-y
6. Feng J, Zhu J, Lv W, Li J, Yan W (2015) Chem Eng J 269:316. https://doi.org/10.1016/j.cej.2015.01.109
7. Wei R, Song W, Yang F, Zhou J, Zhang M, Zhang X, Zhao W, Zhao C (2018) Ind Eng Chem Res 57:8209. https://doi.org/10.1021/acs.iecr.8b01027
8. Satilmis B, Budd PM (2017) J Colloid Interf Sci 492:81. https://doi.org/10.1016/j.jcis.2016.12.048
9. Mustafa S, Khan HM, Shukla I, Shujatullah F, Shahid M, Ashfaq M, Azam A (2011) East J Med 16:253
10. Shinde DR, Tambade PS, Chaskar MG, Gadave KM (2017) Drink Water Eng Sci 10:109. https://doi.org/10.5194/dwes-10-109-2017
11. Huang Q, Liu M, Chen J, Wan Q, Tian J, Huang L, Jiang R, Wen Y, Zhang X, Wei Y (2017) Appl Surf Sci 419:35. https://doi.org/10.1016/j.apsusc.2017.05.006
12. Zhang R-Z, Quan S, Xia M, Wang Q, Zhang W, Yang J-M (2018) J Colloid Interface Sci 525:54. https://doi.org/10.1016/j.jcis.2018.04.039
13. Wei R, Wang J, Zhang H, Han W, Liu X (2017) Polym 9:342. https://doi.org/10.3390/polym9080342
14. Wei R, Tu L, You Y, Zhan C, Wang Y, Liu X (2019) Polym 161:162. https://doi.org/10.1016/j.polymer.2018.12.017
15. Seo M, Kim S, Oh J, Kim S-J, Hillmyer MA (2015) JACS 137:600. https://doi.org/10.1021/ja511581w
16. Yılmaz O, Cheaburu-Yılmaz CN (2018) J Polytech 21(1):19. https://doi.org/10.2339/politeknik.376390
17. Fan L, Zhou Y, Yang W, Chen G, Yang F (2008) Dyes Pigm 76:440. https://doi.org/10.1016/j.dyepig.2006.09.013
18. Wawrzkiewicz M (2012) Ind Eng Chem Res 51:8069. https://doi.org/10.1021/ie3003528
19. Wu J-S, Liu C-H, Chu KH, Suen S-Y (2008) J Membr Sci 309:239. https://doi.org/10.1016/j.memsci.2007.10.035
20. Woo YS, Rafatullah M, Al-Karkhi AFM, Tow TT (2014) Desalin Water Treat 52:4583. https://doi.org/10.1080/19443994.2013.804454
21. Jawad AH, Alkarkhi AFM, Mubarak NSA (2015) Desalin Water Treat 56:161. https://doi.org/10.1080/19443994.2014.934736
22. Jawad AH, Mubarak NSA, Ishak MAM, Ismail K, Nawawi WI (2016) J Taibah Univ Sci 10:352. https://doi.org/10.1016/j.jtusci.2015.03.007
23. Jawad AH, Azharul Islam M, Hameed BH (2017) Int J Biol Macromol 95:743. https://doi.org/10.1016/j.ijbiomac.2016.11.087
24. Kannan N, Sundaram MM (2001) Dyes Pigm 51:25. https://doi.org/10.1016/S0143-7208(01)00056-0
25. Yu Y, Zhuang Y-Y, Wang Z-H (2001) J Colloid Interface Sci 242:288. https://doi.org/10.1006/jcis.2001.7780
26. Şen F, Demirbaş Ö, Çalımlı MH, Aygün A, Alma MH, Nas MS (2018) Appl Water Sci 8:206. https://doi.org/10.1007/s13201-018-0856-x
27. Di Mauro A, Cantarella M, Nicotra G, Pellegrino G, Gulino A, Brundo MV, Privitera V, Impellizzeri G (2017) Sci Rep 7:40895. https://doi.org/10.1038/srep40895
28. Meral K, Metin Ö (2014) Turk J Chem 38:775. https://doi.org/10.3906/kim-1312-28
29. Zhou X, Xu M, Wang L, Liu X (2019) Nanomater 9:1356. https://doi.org/10.3390/nano9101356
30. Fu Z, He C, Li H, Yan C, Chen L, Huang J, Liu Y-N (2015) Chem Eng J 279:250. https://doi.org/10.1016/j.cej.2015.04.146

31. Dulman V, Cucu-Man S-M, Bunia I, Dumitras M (2016) Desalin Water Treat 57:14708. https://doi.org/10.1080/19443994.2015.1065767
32. Amar I, Aharif A, Ali M, Alshareef A, Altohami F, Abdulqdir M, Ahwidi MA (2020) Chem Methodol 4:1. https://doi.org/10.33945/sami/chemm.2020.1.1
33. Yang Q, Ren S, Zhao Q, Lu R, Hang C, Chen Z, Zheng H (2018) Chem Eng J 333:49. https://doi.org/10.1016/j.cej.2017.09.099
34. Flory PJ, Rehner J (1944) J Chem Phys 12:412. https://doi.org/10.1063/1.1723884
35. Flory PJ (1950) J Chem Phys 18:108. https://doi.org/10.1063/1.1747424
36. Bauer DR, Dickie RA (1980) J Polym Sci Pol Phys 18:2015. https://doi.org/10.1002/pol.1980.180181002
37. Slepchuk I, Semeshko OY, Asaulyuk TS, Saribekova YG (2018) Izvestiya vysshikh uchebnykh zavedeniy khimiya khimicheskaya tekhnologiya 61:68. https://doi.org/10.6060/ivkkt.20186107.5670.(inRuss)
38. Ahmed R, Tariq M, Ali I, Asghar R, Noorunnisa Khanam P, Augustine R, Hasan A (2018) Int J Biol Macromol 120:385. https://doi.org/10.1016/j.ijbiomac.2018.08.057
39. Al-saadi TM, Bakr NA, Hameed NA (2014) Int J Eng Techn Res 2(4):191
40. Cao D, Gong S, Shu X, Zhu D, Liang S (2019) Nanoscale Res Lett 14:210. https://doi.org/10.1186/s11671-019-3038-3
41. Pradeeba SJ, Sampath K (2018) J Ovonic Res 14:243
42. Eivazzadeh-Keihan R, Taheri-Ledari R, Khosropour N (2020) ColloidsSurf A Physicochem Eng Asp 587. https://doi.org/10.1016/j.colsurfa.2019.124335.
43. Fu Y, Viraraghavan T (2001) Bioresour Technol 79:251. https://doi.org/10.1016/S0960-8524(01)00028-1
44. Melnyk IV, Tomina VV, Stolyarchuk NV, Bespalko OV, Vaclavikova M (2020) Appl Nanosci 10:2813. https://doi.org/10.1007/s13204-019-01087-1
45. Kotsyuda SS, Tomina VV, Zub YL, Furtat IM, Lebed AP, Vaclavikova M, Melnyk IV (2017) Appl Surf Sci 420:782. https://doi.org/10.1016/j.apsusc.2017.05.150
46. Ye J, Nyobe D, Tang B, Bin L, Li P, Huang S, Fu F, Cai Y, Guan G, Hao X (2020) J Mol Liq 303:112656. https://doi.org/10.1016/j.molliq.2020.112656